Efficient and Robust Plane-Based Boolean Operations on N Meshes

Abstract—Constructive solid geometry (CSG) is widely used for computer aided design and manufacturing. However, boolean operations, which compute the boundary representation of CSG, have been suffered from robustness and efficiency problem for more than three decades. We propose a fast and exact boolean operation method which is unconditionally robust for regular set solids. We notice that among previous works,boolean methods using plane representations (P-reps) of meshes are easy to achieve robustness, but hard to be efficient. On the other hand, methods based on boundary representation (B-reps) of meshes are fast but not robust unless exact arithmetic is applied. Therefore, we choose to combine P-reps with B-reps, which allows us to take the advantages of both. Our method is globally based on B-reps for its efficiency, and P-rep geometry is applied locally to ensure robustness. Comparison experiments with state-of-the-art techniques show that our method is unconditionally exact and robust, while is competitively efficient as non-robust methods.

Index Terms—boolean operations, CSG evaluation, plane-based geometry

1 Introduction

Constructive solid geometry (CSG) has long been a popular modeling tool of computer-aided design and computer-aided manufacturing (CAD/CAM). It constructs complex models by combining primitives using a series of regularized boolean operations [1], [2]: union, intersection and difference. CSG can be converted into the widely-used boundary representation (B-rep) through boolean operations, which is an classical topic with history of over three decades.

In general, there are two major types of boolean algorithms according to how they deal with intersection between primitive meshes. Approximate methods [3], [4], [5] redicretize the intersection areas, fit vertices approximatively and rearrange topology. On the other hand, exact method do not change vertex positions, retain as many input elements (e.g., faces, vertices and topology) as possible. In many applications, exact methods are preferred for their accuracy. Also, using exact methods, the clear mapping between the surface of input and output meshes makes it easier for the inheritance of information like face colors and materials.

However, for exact boolean operation methods, there is always a bargain between robustness and efficiency. Many exact boolean operation methods focus on efficiency. But for robustness, the solutions are either exact arithmetic [6], [7] or trivial workarounds to avoid degenerations, such as setting a tolerance [8], [9] and rotating the primitive with small angles [10]. Methods using exact arithmetic are significantly slower, and workarounds are often case dependent and not reliable. Recently, some methods [11], [12] seek unconditional robustness by avoiding geometry constructions (such as computing new vertex coordinates) and using only predicates. Their key idea is to utilize plane-based representations (P-reps) of meshes instead of boundary representation (B-reps), which comes from the observation of Sugihara and Iri [13] that boolean operations can be performed without geometry constructions if P-reps are used. While these plane-based methods are generally faster than exact arithmetic ones, they still suffer from performance issue because of the complex conversions among different representations. Also, the incoherence between different representations requires extra steps to reconstruct geometry connectivity, leading to extra computation burden and more complex topology.

Inspired by these previous work, we develop an unconditionally robust boolean operation method which is as robust as P-rep-based method and as fast as non-robust B-rep-based method. To achieve this, we embed P-rep information into faces of B-reps, forming hybrid representation of meshes. We avoid geometry constructions throughout our method, and convert all necessary computation into predicates under the hybrid representation. In general, the B-reps information is used for coarse tests and efficient face neighbor query, while P-reps information is for exact geometry computation. During intersection computation, we encode the intersections between meshes into sets of planes and use these planes to perform exact tessellation. After that, we classify each faces in the tessellated meshes using local binary space partition (BSP) trees, which also facilitate the previous plane-based representation to guarantee exactness. In addition, while most previous boolean operations can only deal with two meshes, our method can perform boolean operations with arbitrary meshes in one call, instead of recursively doing incremental boolean operations. In this way, our method could save computation time by avoiding repetitive computation. The experiments show that our method is much faster than existing robust

- *R. Wang and B. Sheng are with the Department of Computer Science and Engineering, Shanghai Jiao Tong University. E-mail:{jhcz,shengbin}@sjtu.edu.cn*
- *X. Jiang is with Autodesk China Research & Development Center. Email: xudong.jiang@autodesk.com*
- *H. Fu is with the School of Creative Media, City University of Hong Kong. Email: hongbofu@cityu.edu.hk*
- *P. Li is with the Department of Mathematics and Information Technology, The Hong Kong Institute of Education. Email: pli@ied.edu.hk*
- *E. Wu is currently a research professor at State Key Lab. of Computer Science, Institute of Software, Chinese Academy of Sciences. Email: ehwu@umac.mo*

exact methods, while only about two times slower than the state-of-art non-robust exact methods.

2 Related Work

Boolean operations have been researched for over three decades since it inception in the 1980s [14], [15]. Previous works can be classified into two categories: exact methods and approximate methods. Exact methods retain vertex positions. Also the topology of the input meshes is preserved as much as possible. The coordinates of intersection points between input meshes are computed by input configurations to construct the topology around intersection. However, the coordinates cannot be represented exactly using fix-precision float-point numbers and the robustness is always a problem. On the other hand, approximate methods rediscretize the input mesh surfaces using techniques such as voxels, octrees and Layered Depth Images. They can reach better performance and robustness, but the loss of geometry information and precision is inevitable.

2.1 Exact Methods

For exact methods, some [7], [8], [10], [16], [17] pursues efficiency but cannot guarantee robustness in degenerate cases. Most of them are implemented by fix-precision float-point arithmetic and numerical errors are inevitable. Douze et al. [10] implemented very efficient method that can handle very large meshes. Also, they can perform non-incremental boolean operations: evaluating the final result mesh of CSG all at once instead of decomposing the CSG into a series of incremental boolean operations. However, their method can neither deal with coplanar cases nor guarantee accuracy of topology. In fact, large CSGs are more complex and more likely to contain degenerate cases, and more vulnerable under numerical errors. Efficiency only is far from being practical.

Many researchers have attempted to solve robustness issue for exact boolean operations using arbitrary precision arithmetic [18], [19], [20], [21], [22] and exact interval computation [9], [23], [24]. However, these methods are too expensive in computation time and memory to be practical for large CSGs. For example, one of the available implementation of robust exact boolean operations method is CGAL's [25] exact-arithmetic implementation [21] of Nef polyhedra [26]. It requires conversions between Nef polyhedra and input mesh data structures during evaluation and is more than 50 times slower than non-robust booleans [11].

2.2 Approximative Methods

Since efficiency, accuracy and robustness are hard to be satisfied at the same time, some method choose to sacrifice accuracy for better efficiency and robustness. Most of such methods are based on conversion to volumetric representations. However, the quality of result mesh depends on the resolution of the volume grid and better quality requires dramatically higher resolution. To accelerate this process, some try to reduce the complexity of the output mesh [27] and others try to preserve non-intersected areas of the input mesh to avoid redundant tessellation [3], [4], [28], [29], [30]. Also, with the development of general-purpose computing on graphics processing units (GPGPU), many of them utilize the grand computation power of graphics hardware for boolean operations. These methods have good performance and are suitable for interactive applications. However, the fundamental problem of approximate methods is owing to grid-depend nature of volumetric calculations: they inevitably suffers from geometric detail loss and unwieldy topology changes.

2.3 Plane-Based Methods

The concept of plane-based representations (P-reps) of polygonal meshes was first described by Sugihara and Iri [13]. P-reps provide essential benefit for boolean operations that no new geometry primitive has to be constructed to obtain the results—they can be composed of a subset of the planes from the input polyhedra. It means the computation can include only geometry predicates, which are much easier to be implemented exactly and robustly. Based on P-reps, Berstein and Fussell [11] combined the P-reps with binary space partition (BSP) trees [31], [32] to develop a boolean operation method which is unconditionally robust under consistent inputs . Compared to B-rep-based methods, their method does not rely on exact arithmetics to be robust. However, the merge of two BSP trees is an $O(mn)$ time complexity process, where m and n are the size of the trees. It makes this method impractical for large meshes. Later, Campen and Kobbelt [12] improved their method by localize BSP operations using an octree. The mesh refinement only takes place locally near intersections, which is much faster than Berstein and Fussell's work.

3 Background and Overview

Our method is designed for boolean operations on arbitrary number of regular triangle meshes [14]. Input meshes are required to be free from self-intersecting, and they are represented with B-reps with geometry connectivity (e.g., halfedge, winged-edge, etc.). Despite of these requirements, our method is robust and not sensitive to topology deficiencies like holes and self-intersections and works correctly if deficiencies are not near the intersection areas between meshes.

3.1 Boolean Numerical Errors

The boolean operation of triangle meshes is in essence a process of face selection. Namely, given a boolean function, it reserves those primitive faces that pass the function and drop the others to generate the final mesh. Unfortunately, for B-rep meshes, not all the input faces can be classified as a whole, since for faces near the intersections, only parts of them belong to the final mesh. Therefore, we need an extra step aiming at detecting intersections between meshes and performing tessellation. Most of the boolean operation methods follow this two-step paradigm, which consists of intersection computation and face classification. So is our method.

The first step is intersection computation. Input faces are tested in pairs to compute their intersections. Each input meshes are tessellated according to the intersection results, making every face be completely inside, outside or on the

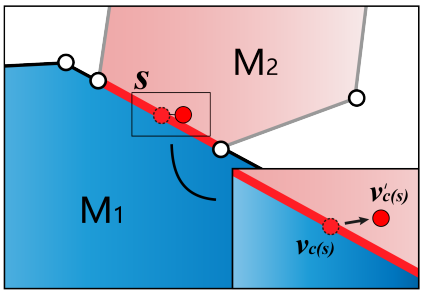

Fig. 1. In the 2D view, face $\boldsymbol{s}$ (the red line segment) from mesh M_2 is on the surface of mesh M_1. However, because we use face barycenter $\boldsymbol{v}_{c(\boldsymbol{s})}$ to compute the indicator, whose coordinates contains round-off error, the point could move to $\boldsymbol{v}'_{c(\boldsymbol{s})}$. Then we might falsely classify $\boldsymbol{s}$ as outside of M_1.

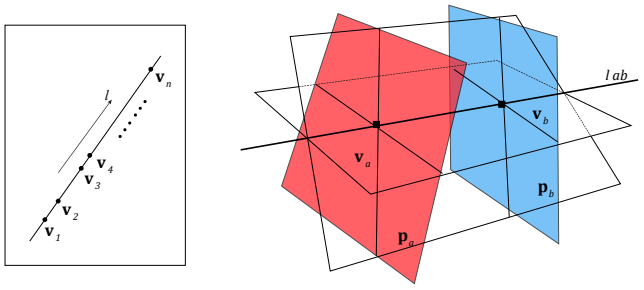

Fig. 2. Geometry configuration of linear ordering of points. Points $\boldsymbol{v}_a$ and $\boldsymbol{v}_b$ are both on line $\boldsymbol{l}_{ab}$. We convert this problem into the plane ordering of $\boldsymbol{p}_a$ and $\boldsymbol{p}_b$ along $\boldsymbol{l}_{ab}$.

boundary of other primitives. The tessellated meshes are what we called *intersection-free meshes*. Unfortunately, under fix-precision float-point arithmetic, intersection tests are error-prone: first, degenerate cases of intersection are hard to detect; second, when there are intersections, new vertices are introduced into the geometry, whose coordinates cannot be exactly represented by fix-precision float-point numbers.

The second step is face classification. We evaluate whether a given face $\boldsymbol{s}$ belongs to the final geometry according to the n-primitive boolean function f :

$$\lambda_f(\boldsymbol{s}) = f(\boldsymbol{\Lambda}(\boldsymbol{s})) = f(\lambda_1(\boldsymbol{s}), \lambda_2(\boldsymbol{s}), \cdots, \lambda_n(\boldsymbol{s})). \quad (1)$$

The parameter $\lambda_i(\boldsymbol{s})$ is space indicator with respect to mesh M_i. To compute $\lambda_f(\boldsymbol{s})$ and classify $\boldsymbol{s}$, one has to know the space indicators with respect to all the primitives ($\boldsymbol{\Lambda}(\boldsymbol{s})$). A space indicator has four conditions: completely inside (*in*), completely outside (*out*), on the boundary with consistent normals (*same*) or opposite normals (*oppo*). The rules of boolean function evaluation are described in [8], [10].

Face classification also suffers from numerical errors. Many methods classify face according to the indicators of its barycenter using point-in-polyhedron test [8], [12]. However, coordinates of barycenters cannot be exactly represented and could generate false classification (illustrated in Fig. 1). What makes the problem worse is that for the large amount of faces and input meshes, many methods [4], [7], [8], [16] take the benefits of the local coherence of indicators, classifying neighboring faces together . Despite of the performance improvement, it can propagate false classification to neighboring faces and lead to wide-range failure.

3.2 Plane-based Geometry

In our method, we avoid numerical errors by embeding P-reps into conventional B-rep-based boolean algorithms and substituting constructions under B-reps with predicates under P-reps. Using P-reps, each face $\boldsymbol{s}$ with n edges is represented by a supporting plane $\boldsymbol{p}_{s,sp}$, where the face lies, and a list bounding planes $\{\boldsymbol{p}^i_{s,b} \mid i = 0, 1, ..., n-1\}$. Each edge

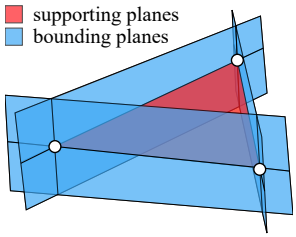

line $\boldsymbol{e}^i_{\boldsymbol{s}}$ is represented by intersection $\boldsymbol{p}_{s,sp} \cap \boldsymbol{p}^i_{s,b}$. Corner vertex $\boldsymbol{v}^i_s$ is represented by $\boldsymbol{p}_{s,sp} \cap \boldsymbol{p}^i_{s,b} \cap \boldsymbol{p}^{(i+1) \bmod n}_{s,b}$. We use Campen et al.'s method [12] for exact conversion of triangles to their P-reps. All geometry predicates are computed using filtering techniques proposed by Shewchuk [33] for both exactness and efficiency.

Other commonly used notations in this paper are presented here. The normal of a plane $\boldsymbol{p}$ is denoted as $\boldsymbol{n}(\boldsymbol{p})$. A line $\boldsymbol{l}$ can be represented by intersection of two planes $(\boldsymbol{p}^0_l \cap \boldsymbol{p}^1_l)$, or in short, $\boldsymbol{l}$: $(\boldsymbol{p}^0_l \cap \boldsymbol{p}^1_l)$. The positive direction of the line $\boldsymbol{l}$ is defined by $\boldsymbol{n}(\boldsymbol{p}^0_l) \times \boldsymbol{n}(\boldsymbol{p}^1_l)$. A point $\boldsymbol{v}$ can be represented by non-trivial plane triples $(\boldsymbol{p}^0_v \cap \boldsymbol{p}^1_v \cap \boldsymbol{p}^2_v)$, or in short, $\boldsymbol{v}$: $(\boldsymbol{p}^0_v \cap \boldsymbol{p}^1_v \cap \boldsymbol{p}^2_v)$.

Plane-based geometry predicates used in our method are mostly well-discussed in previous work [11], [18]. In the following, we focus on two predicates related to sorting, which are designed for our method particularly.

Linear ordering of points

Given an line $\boldsymbol{l}_{ab}$ with two points $\boldsymbol{v}_a$: $(\boldsymbol{p}^0_a \cap \boldsymbol{p}^1_a \cap \boldsymbol{p}^2_a)$ and $\boldsymbol{v}_b$: $(\boldsymbol{p}^0_b \cap \boldsymbol{p}^1_b \cap \boldsymbol{p}^2_b)$ on it, we need to determine the linear order of the two points along $\boldsymbol{l}_{ab}$ (Fig. 2). To solve this problem, we choose one plane not parallel with $\boldsymbol{l}_{ab}$ from the plane representation of each point and convert this problem into linear order of planes, which can be solved by Banerjee et al.'s method [18]. The chosen planes should have the same orientation with $\boldsymbol{l}_{ab}$ (the dot product between plane normal and $\boldsymbol{l}_{ab}$ has to be positive) and unqualified planes have to be flipped.

Circular ordering of lines

During face tessellation, we need to know the which edges are neighboring (Fig. 3), that is, circular ordering of directed lines around a vertex. Lines can be sorted in a divide-and-conquer way based on the relative order of each pair of lines. Therefore, this problem is converted to that given two lines $\boldsymbol{l}_a$ and $\boldsymbol{l}_b$ in a plane $\boldsymbol{p}_0$ and their intersection point $\boldsymbol{v}_{ab}$, compute the circular order of the two lines. We can compute the order by the sign of $\sin\theta_{ab}$, where $\theta_{ab} \in (-\pi, \pi)$ is the angle from $\boldsymbol{l}_a$ to $\boldsymbol{l}_b$ under the top view of $\boldsymbol{p}_0$. The sign of $\sin\theta_{ab}$ is the same as triple product $\boldsymbol{n}(\boldsymbol{p}_0) \cdot (\boldsymbol{l}_a \times \boldsymbol{l}_b)$. However, explicit computing this equation is complicated because both $\boldsymbol{l}_a$ and $\boldsymbol{l}_b$ are implicitly

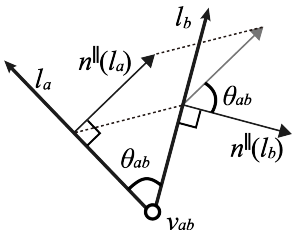

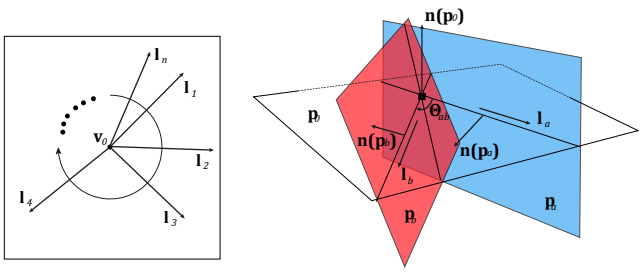

Fig. 3. Geometry configuration of circular ordering of lines. $\boldsymbol{l}_a$: $(\boldsymbol{p}_0 \cap \boldsymbol{p}_a)$ and $\boldsymbol{l}_b$: $(\boldsymbol{p}_0 \cap \boldsymbol{p}_b)$ are within plane $\boldsymbol{p}_0$.

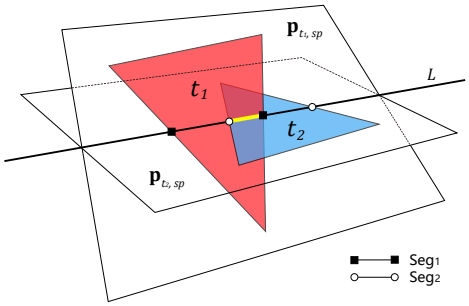

Fig. 4. Seg_1 is the intersection between $\boldsymbol{p}_{t_2,sp}$ and t_1. Seg_2 is the intersection between $\boldsymbol{p}_{t_1,sp}$ and t_2. The intersection between t_1 and t_2, which is the line segment in yellow, is the overlap of Seg_1 and Seg_2.

represented by intersection of planes.

We develop an easier way that requiring no explicit computation of $\boldsymbol{l}_a$ and $\boldsymbol{l}_b$. First, we write the P-reps of two lines as $\boldsymbol{l}_a$: $(\boldsymbol{p}_0 \cap \boldsymbol{p}_a)$ and $\boldsymbol{l}_b$: $(\boldsymbol{p}_0 \cap \boldsymbol{p}_b)$. Then we orthogonally decompose $\boldsymbol{n}(\boldsymbol{p}_a)$ and $\boldsymbol{n}(\boldsymbol{p}_b)$ along $\boldsymbol{n}(\boldsymbol{p}_0)$:

$$\begin{aligned} \boldsymbol{n}(\boldsymbol{p}_a) &= \boldsymbol{n}^{\parallel}(\boldsymbol{p}_a) + \boldsymbol{n}^{\perp}(\boldsymbol{p}_a) \\ \boldsymbol{n}(\boldsymbol{p}_b) &= \boldsymbol{n}^{\parallel}(\boldsymbol{p}_b) + \boldsymbol{n}^{\perp}(\boldsymbol{p}_b) \end{aligned} \tag{2}$$

Here superscript '$\parallel$' means the projection on $\boldsymbol{p}_0$ and '$\perp$' means orthogonal to $\boldsymbol{p}_0$. As we know $\boldsymbol{n}^{\perp}(\boldsymbol{p}_a)$ and $\boldsymbol{n}^{\perp}(\boldsymbol{p}_b)$ are both parallel to $\boldsymbol{n}(\boldsymbol{p}_0)$, we get:

$$\boldsymbol{n}(\boldsymbol{p}_0) \cdot (\boldsymbol{n}(\boldsymbol{p}_a) \times \boldsymbol{n}(\boldsymbol{p}_b)) = \boldsymbol{n}(\boldsymbol{p}_0) \cdot (\boldsymbol{n}^{\parallel}(\boldsymbol{p}_a) \times \boldsymbol{n}^{\parallel}(\boldsymbol{p}_b)). \tag{3}$$

By observation we find that the angle between $\boldsymbol{n}^{\parallel}(\boldsymbol{p}_a)$ and $\boldsymbol{n}^{\parallel}(\boldsymbol{p}_b)$ is exactly θ_{ab}. So the sign of the right side of equation 3 is exactly the sign of $\sin\theta_{ab}$. It means we have the following nice conclusion:

$$sign(\sin\theta_{ab}) = sign(\boldsymbol{n}(\boldsymbol{p}_0) \cdot (\boldsymbol{n}(\boldsymbol{p}_a) \times \boldsymbol{n}(\boldsymbol{p}_b))) \tag{4}$$

Since all the three vectors on the right side are already explicitly represented, we only have to evaluate the sign of an 3×3 matrix and avoid complicated arbitrary precision float-point arithmetic.

3.3 Method Overview

There are generally three steps in our method. The first step is to compute intersections between each triangle face pairs. After that, the input meshes are tessellated into intersection-free meshes according to these intersections. The last step is to classify each face and generate the final result mesh.

3.3.1 Intersection computation

In this step, we only compute intersections between triangle pairs. The triangle-triangle intersection test is largely based on Möller's algorithm [34] for its efficiency. However, conventional implementation of Möller's algorithm using vertex-based geometry brings numerical errors. Therefore, we integrate P-rep into Möller's algorithm. All intersection points and line segments are represented using planes to avoid explicitly computing the coordinates. Also, we carefully deal with degenerate cases of triangle intersections, including point intersections, edge intersections and coplanar situations. In addition, octree is used to speed up the whole process. Details are provided in §4.

3.3.2 Deferred tessellation

Once all intersections between triangles are detected, we need to tessellate the input meshes and construct the intersection-free meshes. In many methods like [16], constraint Delaunay triangulation (CDT) is applied to perform tessellation. However, for a CSG with more than two meshes, intersections may overlap or intersect with each other, and cannot be used for constraints of CDT directly. In addition, as our intersections are represented by planes, implementation of CDT are complex and inefficient, as most CDT algorithms (e.g. [35], [36]) is not designed to handle planes and requires explicit coordinates. Therefore, we first perform intersection refinement to resolve intersecting intersections. After that, we construct a graph-like structure suitable for P-rep intersections, called *tess-graph*, to guide the exact tessellation of each face. After all faces are tessellated, we get our intersection-free meshes. Details are shown in §5.

3.3.3 Face classification

This step is to choose faces from the intersection-free meshes to generate the final mesh. However, literally computing the indicator vector of each face is unacceptably slow for large CSGs. We utilize the geometry connectivity stored in B-reps to propagate indicators in a flood-filling manner. In addition, many methods use barycenters of faces together with point-in-polyhedra test for face classification, which is not exact nor robust with fix-precision float-point arithmetics. Different from them, we classify faces based on the classification results of exactly represented vertices, including input vertices and newly introduced intersection vertices, and carefully deal with coplanar conditions to ensure topology consistency. Details will be shown in §6.

4 Intersection Computation

In this step, intersections between faces are computed through triangle-triangle intersection test. We adopt Möller's algorithm [34] on account of its efficiency and simplicity. However, a naive implementation of Möller's algorithm can introduce numerical errors and may fail to produce correct results. Therefore, we integrate plane-based geometry to make it exact. In the following, we first introduce our space division strategy to reduce the number of intersection test. Then we make a quick review

of Möller's algorithm, and discuss the way to embed plane-based geometry. After that, we discuss how to deal with degenerate cases.

4.1 Space Division

As intersection detection is performed between each pair of faces, localization is necessary for large C-SGs to reduce the number of testing pairs. We use the adaptive octree for this purpose. Our implementation is akin to the implementation in Ogayar et al.'s method [16]. Intersection between triangle faces and octree nodes are efficiently detected using the separating axis theorem [37]. Octree leaves are classified into two types: if all faces that intersect a leaf belong to the same mesh, we call it a *normal cell*. Otherwise, it is a *critical cell*, within which the following intersection computation is performed.

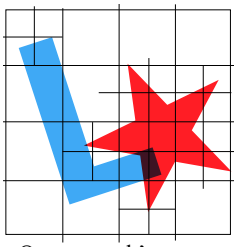

Ogayar et al.'s octree

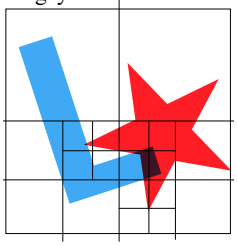

our octree

The difference between our octree and Ogayar et al.'s is that we do not subdivide any normal cell no matter how many faces it contains. This is because subdividing normal cells benefits only the point-in-polyhedron test [38], which seldom uses in our method. This simplification can save much computing time, especially when intersections between primitives are not complex and located in small regions.

4.2 Möller's Vertex-Based Method

Möller's algorithm computes the intersection between two triangles t_1 and t_2 in three steps as shown in Fig. 4:

1) An early rejection is performed by testing whether t_1 intersects $\boldsymbol{p}_{t_2,sp}$, the supporting plane of t_2. The same test is also done between t_2 and $\boldsymbol{p}_{t_1,sp}$.
2) The intersection between t_1 and $\boldsymbol{p}_{t_2,sp}$, denoted as Seg_1, and the intersection between t_2 and $\boldsymbol{p}_{t_1,sp}$, denoted as Seg_2, are separately computed .
3) The intersection between t_1 and t_2 is determined by computing the overlap between Seg_1 and Seg_2 .

The non-robustness of this algorithm is from computing the coordinates of intersection vertices, which is the end points of $Seg1$ and $Seg2$. Although implementation with arbitrary precision arithmetic produces exact coordinates, it is too costly for boolean operations of large CSG. We use plane-based geometry to solve this problem by implicitly representing intersections with planes.

4.3 Plane-Based Intersection

Given a triangle face t, it is firstly converted to its P-rep: a supporting plane $\boldsymbol{p}_{t,sp}$ surrounded by three bounding planes $\{\boldsymbol{p}^i_{t,b} |\ i = 0,1,2\}$. We integrate the plane-based geometry into each of the tree steps of Möller's algorithm as following:

1) The basic subroutine of the first step is to compute the orientation of of a face with respect to vertices of the other face. We find that since the exact coordinates of each triangle vertices are known, we can compute the point-plane orientation using vertex-based geometry predicates. This allow us to perform this early rejection efficiently.

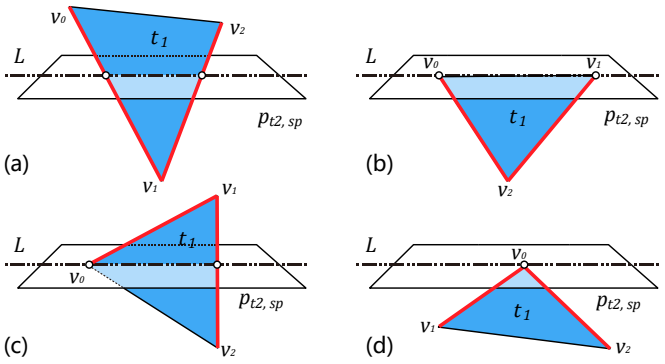

Fig. 5. We denote the signed distance from point v_i to plane $\boldsymbol{p}_{t_2,sp}$ as d_i. All the four conditions of intersection between t_1 and $\boldsymbol{p}_{t_2,sp}$ are: (a) $d_0 \cdot d_2 < 0$, $d_1 \cdot d_2 < 0$; (b) $d_0 = 0$, $d_1 = 0$, $d_2 \neq 0$; (c) $d_0 = 0$, $d_1 \cdot d_2 < 0$; (d) $d_0 = 0$, $d_1 \cdot d_2 > 0$. End points of Seg_1 are intersections between $\boldsymbol{p}_{t_2,sp}$ and related edges of t_1 (red bold lines).

2) If t_1 and t_2 are not coplanar, the end points of Seg_1 and Seg_2 can be implicitly represented by plane triples. Take Seg_1 as an example. Seg_1 is the intersection between t_1 and $\boldsymbol{p}_{t_2,sp}$ and the end points of Seg_1 are intersections between $\boldsymbol{p}_{t_2,sp}$ and edges from t_1 (denoted as $\boldsymbol{e}^i_{t_1}, i \in \{0,1,2\}$). Because $\boldsymbol{e}^i_{t_1}$ can be represented as $\boldsymbol{p}_{t_1,s} \cap \boldsymbol{p}^i_{t_1,b}$, the end points of Seg_1 can be represented in the form of $\boldsymbol{p}_{t_2,sp} \cap \boldsymbol{p}_{t_1,sp} \cap \boldsymbol{p}^i_{t_1,b}$. In Fig. 5, we list all possible intersecting situations between t_1 and $\boldsymbol{p}_{t_2,sp}$ and the corresponding $\boldsymbol{e}^i_{t_1}$. The coplanar situation will be discussed later in §4.5.
3) The intersection between t_1 and t_2 is the overlap area of Seg_1 and Seg_2. It can be easily computed by sorting the end points of Seg_1 and Seg_2 along the line $\boldsymbol{l}$: $\boldsymbol{p}_{t_1,sp} \cap \boldsymbol{p}_{t_2,sp}$. Because end points are all represented using plane triples, we can use the linear order of points discussed in §3.2 to sort.

Each time an intersection is computed, two intersections are generated (one for each triangle) and the newly generated vertices are added into meshes. To avoid repetitive vertices in the final result, we perform vertex repetition elimination in this step, merging coincident vertices even if they come from different input meshes. Because we use P-reps, the comparison of vertices is exact.

4.4 Plane-Based Intersection Representation

In our method, intersection on triangle t is stored as $\mathfrak{I}$: $\{T, \boldsymbol{P}_{ext}, (\boldsymbol{P}_0, \boldsymbol{P}_1), \mathcal{N}\}$, which is called plane-based intersection representation (PBI-rep, see Fig. 6). The first component T indicates which triangle $\mathfrak{I}$ lies on. $\boldsymbol{P}_{ext}$ indicates $\mathfrak{I}$ lies on $\boldsymbol{P}_{ext}$, which also means it lies on line $\boldsymbol{p}_{t,sp} \cap \boldsymbol{P}_{ext}$. The two end points of $\mathfrak{I}$ are $\boldsymbol{p}_{t,sp} \cap \boldsymbol{P}_{ext} \cap \boldsymbol{P}_0$ and $\boldsymbol{p}_{t,sp} \cap \boldsymbol{P}_{ext} \cap \boldsymbol{P}_1$. The last component $\mathcal{N}$ represents the neighborhood of the intersection $\mathfrak{I}$. It indicates $\mathfrak{I}$ is intersection of triangle t with $\mathcal{N}$ from other mesh, where $\mathcal{N}$ can be either a face or a set of faces sharing the same edges.

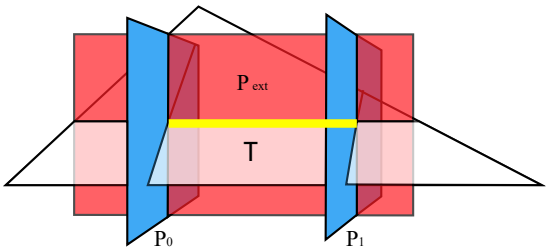

Fig. 6. The geometry meaning of planes in a PBI-rep. The yellow line segment is the represented intersection.

For example, two triangle faces t_1 and t_2 from mesh M_i and M_j intersect. Then it generates two intersections— $\mathfrak{I}_{12}$ on t_1 and $\mathfrak{I}_{21}$ on t_2. For $\mathfrak{I}_{12}$ on t_1, $T = t_1$ and $\boldsymbol{P}_{ext} = \boldsymbol{p}_{t_2,sp}$. The third component is boundary planes from t_2 which has already been discussed in §4.3. The last component is $\mathcal{N} = t_2$. Sometimes intersections may lie on the mesh edges instead of faces (Fig. 7), which is called 'edge intersection'. In that case, the second component of neighborhood is a set of adjacent faces. We postpone the discussion of edge intersection to §4.5.

4.5 Degenerate Case Handling

While two triangles, if intersecting, intersect on a line segment in most situations, they can also intersect on a point or a convex area (coplanar case). Even if the intersection is a line segment, the intersection can be on triangle edges. These degenerate situations prevent us from performing robust boolean operations. In this section, we offer simple but effective way to deal with all these degenerations, which conceals the complexity of intersections and simplifies later processing.

4.5.1 Point intersection

If two triangles intersect on a single point (e.g., Fig. 5d), the intersection cannot be represented using our four-component description since the line segment collapses into a single point. In these cases, we simply add the intersection point into the related triangles to guarantee correct tessellation. No intersection is introduced.

4.5.2 Edge intersection

When intersection line segment lies on the edge of face, we call it *edge intersection*. The space near edge intersection is divided by faces around the intersected edge (typically two faces for a manifold edge), instead of just one face. Therefore, the neighborhood of the related intersection is a set of faces instead of a single one. For example, in Fig. 7, the neighborhood of the intersection on t_1 is $\{t_2, t_2^*\}$.

Another thing needs to be noticed is that there will be repetitive detection of edge intersections. For example, in Fig. 7a, the same intersection on t_1 will be detected twice because t_1 intersect both t_2 and t_2^* in exactly the same intersection. We solve this duplication together with other interactions among different intersections in §5. We also call such t_2 and t_2^* as *companion triangles* in an edge intersection because they share the same edge intersection. This concept will be referred again in the discussion of coplanar cases.

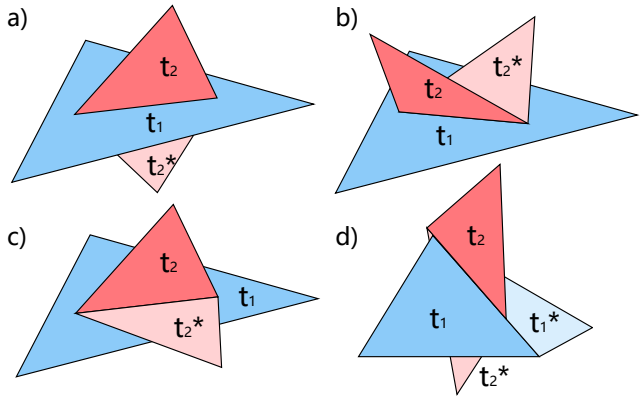

Fig. 7. Different conditions of edge intersection. Triangle faces t_1 and t_1^* are companion faces. Triangle faces t_2 and t_2^* are companion faces. a) t_2 and t_2^* are in different sides of t_1. b) t_2 and t_2^* are in the same side of t_1. c) t_2^* is coplanar with t_1. d) Both t_1 and t_2 have companion faces: the intersection is edge intersection for both t_1 and t_2 (instead of only for t_2 is previous three conditions).

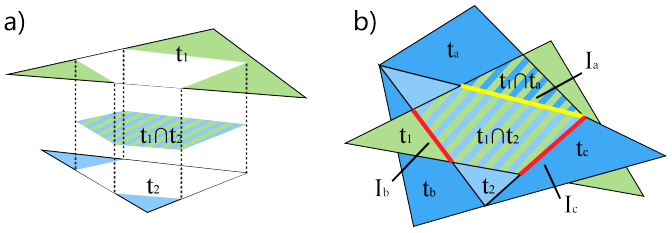

Fig. 8. a) Coplanar cases, t_1 and t_2 intersect in 2D, dividing each other into two areas—a convex overlapping area and exclusive parts. b) The possible configurations of the companion faces. The blue triangles are from the same mesh. For $\mathfrak{I}_a$, the companion triangle t_a is coplanar with the t_1. Therefore, the overlap areas ($t_1 \cap t_a$ and $t_1 \cap t_2$) do not need to be split by the yellow edge during tessellation, thus $\mathfrak{I}_a$ is invalid. For $\mathfrak{I}_b$ and $\mathfrak{I}_c$, the companion faces are not coplanar, so these intersection can be recorded during intersection test between t_1 and t_a or t_1 and t_b. In any situation, there is no need to record the intersection between t_1 and t_2.

4.5.3 Copalnar

Consider two triangle faces $t_1 \in M_x$ and $t_2 \in M_y$ intersect within a common plane. Both t_1 and t_2 will divide each other into two areas—a convex overlapping area and exclusive parts (Fig. 8a). Apparantly, if we tessellate both t_1 and t_2 according to the boundary of overlapping area, we can guarantee that the tessellated meshes are intersection-free. Many previous methods [7], [8] use this method to guarantee topology correctness. However, in our method, we do not test whether t_1 and t_2 really intersect in 2D once we find they are coplanar. We treat coplanar situations as they do not intersect at all. In this way, we simplify our method, making it more robust and fast, while doing no harm to the topology correctness.

We find that each intersection line segment in 2D is part of the edges from input meshes. That means we can view 2D intersection as a special case of edge intersection. The only difference is that there can be up to three edge intersections in one 2D intersection (red and yellow line segments in Fig. 8b). As we have discussed, edge intersection will be detected twice. That means we can rely on the companion triangle faces to detect intersections.

However, if the companion triangles are also coplanar, neither of the two triangles will record the intersection. Fortunately, in this case, the intersection is not valid. The word 'valid' means the intersections will appear as an edge in the final mesh, thus is necessary to put into tessellation. Supposing the intersection $\mathcal{I}$ is on t_1, this definition equals to:

$$\lambda_f(\boldsymbol{v}_i) \neq constant, \boldsymbol{v}_i \in \boldsymbol{U}(\mathcal{I}) \cap M_x \quad (5)$$

, where f is the CSG function, and $\boldsymbol{U}(\mathcal{I})$ is the the neighborhood of $\mathcal{I}$ in $\mathbb{R}^3$. This inequation indicates the space near $\mathcal{I}$ on mesh M_x have different classification and must be split according to $\mathcal{I}$. However, in most time, the validation of intersection is not known until classification stage, because we have to know the indicator of each point in $\boldsymbol{U}(\mathcal{I}) \cap M_x$. Fortunately, if companion face of t_2 is coplanar with t_2, both sides of $\mathcal{I}$ on t_1 have the same indicator $\lambda_y = on$ and thus the same λ_f. It means $\mathcal{I}$ is invalid and we do not need to record it.

5 Deferred Tessellation

After intersection computation, tessellation is performed on each intersecting triangle face to generate the intersection-free meshes. We call this step as deferred tessellation because the tessellation happens until all valid intersections are computed, instead of clipping triangle incrementally by each intersection.

Ogayar-Anguita et. al. [16] use Constrained Delaunay Triangulation (CDT) to perform deferred tessellation. They treat triangle faces as convex triangulation zones and intersections as constraints. Our first try is to implement a robust plane-based CDT. However, CDT algorithms [35], [39] require coordinates projection or intersection detection between arbitrary connections of vertices within triangulation zone, which are difficult to be implemented under P-reps. From another perspective, CDT contains geometry constructions—new edges are generated to guarantee each subface is a triangle (see Fig. 9d), which is not preferred in our method. Moreover, when there are more than two primitives, simply applying CDT omits the complexity of intersections between meshes—the intersections may intersect each other, introducing new vertices and splitting original intersection line segments (see Fig. 9a). This breaks the assumption of most CDT algorithms and may lead to incorrect output topology.

To solve these problems, we first perform intersection refinement to eliminate any crossing or overlapping between intersections. After that, we perform conservative tessellation based on *tess-graph*, ensuring unconditional topology correctness. An tess-graph is a graph-like description of intersections on a certain face. The word 'conservative' means we do not add any new edge during tessellation, which do not guarantee the subfaces are triangles.

5.1 Intersection Refinement

The intersection vertices are not only introduced by intersection between an edge and a triangle, but also introduced by intersections of three triangles. In order to find all intersection vertices, it is not enough by only triangle-triangle intersection tests. Thus, we have to refine these triangle-triangle intersections before the real tessellation.

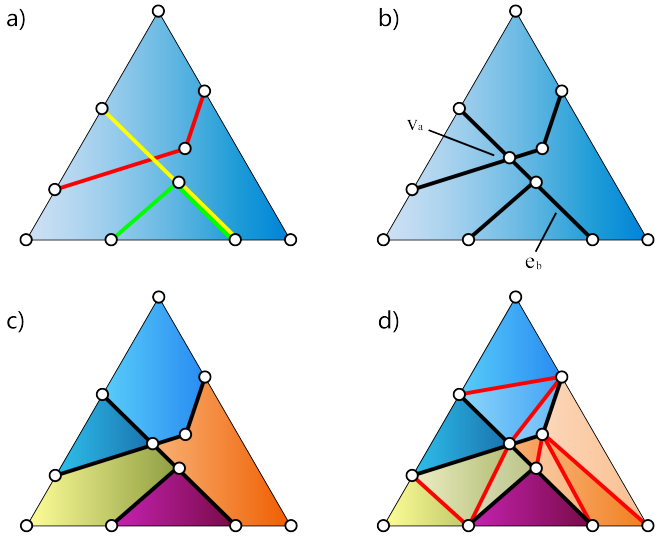

Fig. 9. a) Different colors indicate the intersections are from different meshes. The yellow intersection and the red intersection intersect at a point. Also, the yellow intersection overlap with the green intersection. b) After refinement, we introduce a new vertex $\boldsymbol{v}_a$, and merge overlapping intersections into one edge $\boldsymbol{e}_b$. c) Our tessellation does not guarantee to obtain triangles. d) If triangulation is performed, new edges (red lines) are introduced and we cannot give the precise plane-based representation for these new edges.

Intersection refinement is performed in a local scope. For each intersecting face t, we collect all intersections on t as a set $\boldsymbol{\Gamma}(t)$ and refine them together. We also include the three edges of t into $\boldsymbol{\Gamma}(t)$, since edges also participate in tessellation. In $\boldsymbol{\Gamma}(t)$, edges are represented as PBI: the neighborhood $\mathcal{N}$ of edges are set as N/A because they do not have a neighborhood. Other PBI-rep components can be determined by the P-reps of edges. The refinement on $\boldsymbol{\Gamma}(t)$ is done using only plane-based geometry predicates by the following three steps:

Coincidence elimination We merge coincidence intersections which have the same end points. Intersections are undirected so intersections with inverse end points are also coincident. The PBI-rep of the merging intersection is inherited from either of the old one's except the neighborhood component. The new neighborhood is the union of the merged ones', meaning the intersection has two (or more) neighborhoods.

Cross and overlap resolving After the process of two previous steps, there are no overlapping intersections in $\boldsymbol{\Gamma}(t)$. We check whether any pair of intersections cross or overlap (collinear) each other. New vertices might be introduced in this step. The definition of *cross* does not include the situation that two intersections share one

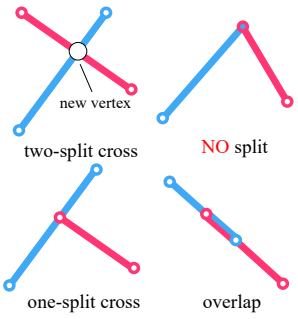

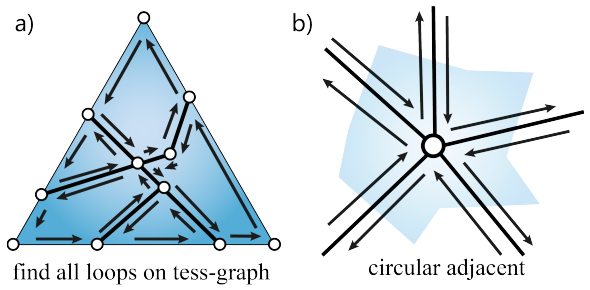

Fig. 10. a) We find all valid loops on tess-graph to tesselate a triangle. The direction of loops have to be coherent with the triangle normal (assume the normal points to the outside of paper). b) Each circular adjacent edge pair is an angle of the tessellated polygon.

end point, since no splitting is required in this situation. When there is crossing or overlapping, at least one of the intersections have to be split. Because one intersection may may 'touch' more than one other intersections, the splitting is deferred until all splitting points are found. The subroutine linear order of points (§3.2) is used to sort these splitting points along the splitting intersection. The PBI-reps of split segments inherit their father's except the $\boldsymbol{P}_0, \boldsymbol{P}_1$, which identifies the P-reps of end points*.

Coincidence elimination (again) Unfortunately, the overlap resolving may bring new coincident intersections in overlap cases. Therefore the first step is run again in the final step.

5.2 Tessellation by Tess-Graph

So far, intersections are only independent data that store the coordinates and neighbourhood information. To perform tessellation and extract subfaces, we need to organize them to reveal the topology. We use tess-graph for this purpose. A tess-graph is the graph description of the tessellated face topology. For each face to be tessellated, we construct a tess-graph according to the refined intersections. Nodes of tess-graph represent end points of intersections and undirectional connections between nodes represent intersections. The construction of tess-graph is straightforward and the reader will not have problem filling the details.

After we have tess-graph, we tessellate face and extract subfaces according to it. This is done by extract valid loops on tess-graph. A valid loop must satisfy two criterions: 1) the direction of loops should be coherent with the face normal, and 2) consecutive connections on the loop should be adjacent by circular order. Each valid loop corresponds to a intersection-free face. After we find out all valid loops on tess-graph, we finish tessellating the corresponding face (see Fig. 10). To facilitate the later process, we also store neighborhood information into the edges of the new faces. The neighborhood information is inherent from the corresponding intersections. When all faces are tessellated, meshes are intersection-free.

6 Face Classification

We traverse each face in the intersection-free meshes, and classify which one belongs to the final mesh. Classification is done by evaluating the indicator vector $\boldsymbol{\Lambda}$ of each face. The basic idea of our classification method is to utilize the space coherence of face indicator vectors to share the classification results among neighboring faces. Also, because we store the neighborhood information in the edges which intersect other meshes, the search space of point-in-polyhedron test is limited to only a few faces. It makes the indicator computation very fast. Finally, by using P-reps, our classification method is exact can deal with any degenerate cases.

The space coherence of indicator vectors means neighboring faces may have the same indicator vector, or most components of indicator vectors. Therefore, we start from a seed face $\boldsymbol{s}_0$ with its indicator vector $\boldsymbol{\Lambda}(\boldsymbol{s}_0)$ known, and propagate to other faces in a flood-filling manner. The trace of indicator propagation is:

$$\boldsymbol{s}_0 \rightarrow \boldsymbol{s}_1 \rightarrow \boldsymbol{s}_2 \rightarrow \boldsymbol{s}_3 \rightarrow \ldots \tag{6}$$

Our intersection-free meshes facilitate this process by accelerating the indicator propagation. Given adjacent faces $\boldsymbol{s}_1$ and $\boldsymbol{s}_2$, it is straightforward to know whether $\boldsymbol{\Lambda}(\boldsymbol{s}_1)$ and $\boldsymbol{\Lambda}(\boldsymbol{s}_2)$ are different. The two indicator vectors are the same unless the shared edge $\boldsymbol{e}_{12}$ lies on the boundary of some other meshes, which means there is neighborhood information, say, $\mathfrak{N}(\boldsymbol{e}_{12}) = \{\mathcal{N}_k\}$, stored on $\boldsymbol{e}_{12}$. Noted that here we use $\mathfrak{N}$ to indicate that there may be more than one neighborhood for the edge (see §5.1). The neighborhood information indicates which components of indicator vector differ between $\boldsymbol{s}_1$ and $\boldsymbol{s}_2$. If there is a neighborhood from mesh M_x, the x^{th} indicators $\lambda_x(\boldsymbol{s}_1)$ and $\lambda_x(\boldsymbol{s}_2)$ differ and can be computed efficiently and exactly according to the neighborhood. We outline our classification method in Algorithm 1.

Algorithm 1 Fast Face Classification

Input: Intersection-free hybrid meshes, boolean function f
Output: Classification $f(\boldsymbol{\Lambda}(\boldsymbol{s}_i))$ for all faces $\boldsymbol{s}_i$

```
Select a proper seed face s_0
Compute the seed indicator vector Λ(s_0)
PROPAGATE( s_0 , Λ(s_0))

function PROPAGATE( s , Λ(s))
    Compute f(Λ(s))
    for each neighboring face s_{s,i} do
        if s_i has been classified then
            continue
        end if
        if there are PBI-reps J_k on e(s_{s,i}, s) then
            compute Λ(s_{s,i}) by Λ(s) and J_k
            PROPAGATE( s_{s,i} , Λ(s_{s,i}))
        else
            PROPAGATE( s_{s,i} , Λ(s))
        end if
    end for
end function
```

6.1 Indicator Propagation

Meshes consist of vertices, edges and faces. Classification is required to perform on the face level. However, polyhedron-in-out test is performed based on points. Gaps exist between the them. Conventionally, face barycenter is used to

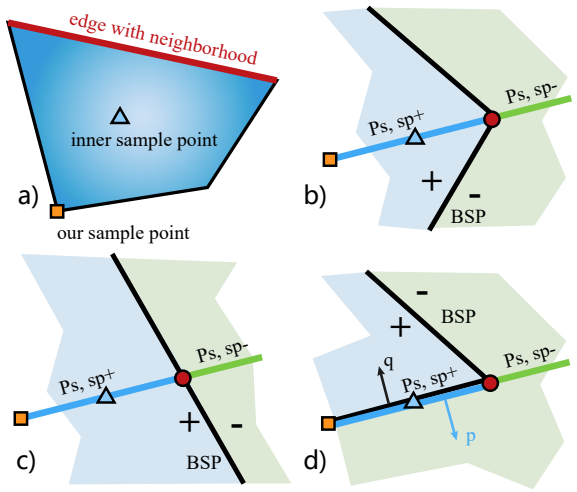

Fig. 11. a) Because inner sample point includes geometry construction, we choose the face vertex (orange one) instead to compute the face indicator. b-d): Different situations of classification. The simple structure of neighborhood BSP guarantees the same classification result of the points on $\boldsymbol{p}^{+}_{\boldsymbol{s},sp}$. In d), the classification result is on so we need to determine the orientation by the normal of BSP splitting plane q and the face normal p. In this condition, the indicator should be $oppo$ since p and q are opposite.

compute the indicator of the whole face. This is because in intersection-free meshes, face is classified as a whole, and every face inner point will have the same indicator as the face's. However, the computation of inner point coordinates requires geometry construction, which introduces errors without exact arithmetic. Therefore, we use the face (or subface) vertices instead, whose exact representations are known, for indicator computation.

However, there are two gaps between face indicator and face vertex indicator. First, the indicator of vertex does not always equal to indicator of face. Second, face indicator has two extra classes in on case—$same$ and $oppo$, because the face has its orientation.

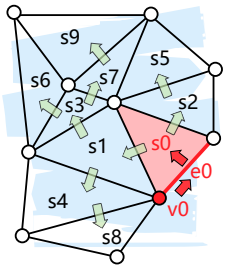

To overcome the gaps, we rewrite our indicator trace (6) in finer granularity. In the beginning, we start from a seed vertex $\boldsymbol{v}_0$ on seed face $\boldsymbol{s}_0$. We assume indicator vector $\boldsymbol{\Lambda}(\boldsymbol{v}_0)$ is known. Then we use $\boldsymbol{\Lambda}(\boldsymbol{v}_0)$ to compute $\boldsymbol{\Lambda}(\boldsymbol{s}_0)$. In addition, we add an optional edge layer into the trace. Then it changes to:

$$\boldsymbol{v}_0 \rightarrow \boldsymbol{e}_0 \rightarrow \boldsymbol{s}_0 \rightarrow (\boldsymbol{e}_1) \rightarrow \boldsymbol{s}_1 \rightarrow (\boldsymbol{e}_2) \rightarrow \boldsymbol{s}_2 \rightarrow \dots \quad (7)$$

, where $\boldsymbol{v}, \boldsymbol{e}$ means vertex and edge respectively. The bracket here means propagating to edge is optional because if the edge does not contain neighborhood information, the indicators on the two side are the same and we do not need to propagate to the edge. We find that there are three kinds of basic operations in the trace: $\boldsymbol{v_e} \rightarrow \boldsymbol{e}$, $\boldsymbol{e_s} \rightarrow \boldsymbol{s}$ and $\boldsymbol{s} \rightarrow \boldsymbol{e_s}$, where $\boldsymbol{v_e}$ means the end point of $\boldsymbol{e}$, and $\boldsymbol{e_s}$ means the edge of $\boldsymbol{s}$.

Given the partial order $on \succ in$ and $on \succ out$, our key observation is that the following relation always stands for indicators within intersection-free meshes:

$$\lambda_k(\boldsymbol{v_{e_s}}) \succeq \lambda_k(\boldsymbol{e_s}) \succeq \lambda_k(\boldsymbol{s}) \quad (8)$$

, where $\lambda_k(x)$ means the indicator of x against a certain primitive M_k. This relation can be inferred from continuous space assumption and the definition of intersection-free mesh*. It tells us when we perform $\boldsymbol{v_e} \rightarrow \boldsymbol{e}$ and $\boldsymbol{e_s} \rightarrow \boldsymbol{s}$, from low-dimension to high-dimension, we decide whether the on indicator changes to in or out or remains on. When we perform $\boldsymbol{s} \rightarrow \boldsymbol{e_s}$, we decide whether in and out indicators change to on. In addition, considering the orientation of face, we also need to figure out whether the on indicators changes to $same$ or $oppo$ during $\boldsymbol{e_s} \rightarrow \boldsymbol{s}$ operation.

$\boldsymbol{s} \rightarrow \boldsymbol{e_s}$ We need to find which indicators change to on. We known when $\lambda_k(\boldsymbol{e_s}) = on$, there will be neighborhood information related to mesh M_k stored on $\boldsymbol{e_s}$. Therefore, in this operation, all we need is to traverse over all neighborhoods of $\boldsymbol{e_s}$ and change corresponding indicators to on.

$\boldsymbol{e_s} \rightarrow \boldsymbol{s}$ From eq. 8, we know if $\lambda_k(\boldsymbol{e_s}) \neq on$, then $\lambda_k(\boldsymbol{e_s}) = \lambda_k(\boldsymbol{s})$. On the other hand, when $\lambda_k(\boldsymbol{e_s}) = on$, we figure out $\lambda_k(\boldsymbol{s})$ using neighborhood information related to M_k. The neighborhood related to M_k can be either a face or a set of faces from mesh M_k. We can build a trivial BSP [31] with these faces. The BSP can be used to compute $\lambda_k(\boldsymbol{s})$ if we can sample a point from $\boldsymbol{s} \cap \boldsymbol{U}(\boldsymbol{e_s})$, where $\boldsymbol{U}(\boldsymbol{e_s})$ is the neighborhood space of $\boldsymbol{e_s}$. Unfortunately, we cannot guarantee to find such a point with precise coordinates.

However, we notice that our BSP is constructed from a single face or a set of faces sharing the same edge. Such BSP is so simple that indicators λ_k of all points on the half plane $\boldsymbol{p}^{+}_{\boldsymbol{s},sp}$ are the same. Here $\boldsymbol{p}^{+}_{\boldsymbol{s},sp}$ is half of the supporting plane of $\boldsymbol{s}$ that on the positive side of bounding plane $\boldsymbol{p}^{\boldsymbol{e_s}}_{\boldsymbol{s},b}$ (see Fig. 11). Since $\boldsymbol{p}^{+}_{\boldsymbol{s},sp} \cap \boldsymbol{s} \neq \varnothing$, we can compute $\lambda_k(\boldsymbol{s})$ by figuring out $\lambda_k(\boldsymbol{v}_x, \boldsymbol{v}_x \in \boldsymbol{p}^{+}_{\boldsymbol{s},sp})$. For polygons, there is at least one corner point on $\boldsymbol{p}^{+}_{\boldsymbol{s},sp}$, whose exact coordinates are known. Then that corner point is used as the $\boldsymbol{v}_x$. Also, we assign each BSP splitting plane a normal by the normal of triangle it contains, by which we can decide the orientation ($same$ or $oppo$) when $\lambda_k(\boldsymbol{s}) = on$.

$\boldsymbol{v_e} \rightarrow \boldsymbol{e}$ If $\lambda_k(\boldsymbol{v_e}) = on$, we first check whether $\lambda_k(\boldsymbol{e}) = on$ by checking whether there is neighborhood information related to M_k on $\boldsymbol{e}$. If not, we need to find where $\boldsymbol{v_e}$ lies on M_k. It is straightforward since the intersection-free meshes contains geometry connectivity. The $\boldsymbol{v_e}$ may lie on a vertex, an edge or a face. We can see this information as the vertex version of neighborhood information, and the same BSP-based classification method is used as in $\boldsymbol{e_s} \rightarrow \boldsymbol{s}$ to determine the high dimension indicator $\lambda_k(\boldsymbol{e})$. We use the other end point $\boldsymbol{v}'_{\boldsymbol{e}}$ to be the sample point for the BSP classification.

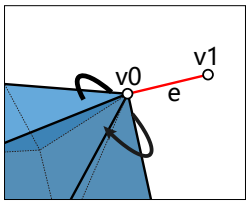

vertex neighborhood

6.2 Acceleration by Caching

If the CSG tree is large with hundreds of primitive nodes, computing $\lambda_f(\boldsymbol{s}_i)$ from $\boldsymbol{\Lambda}(\boldsymbol{s}_i)$ for every face $\boldsymbol{s}_i$ can be costly. Thanks to the indicator space coherence, we can save the

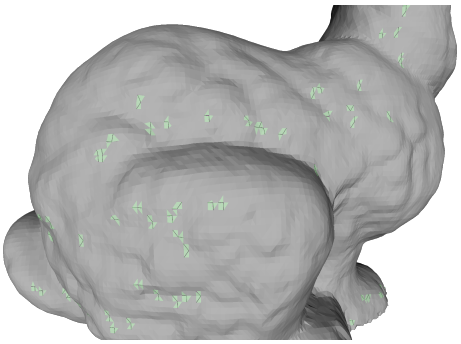

Fig. 12. Even after perturbation, the self-union of *bunny* under QuickCSG still suffers from topology problem. The green faces are boundary faces which indicating topology deficiencies.

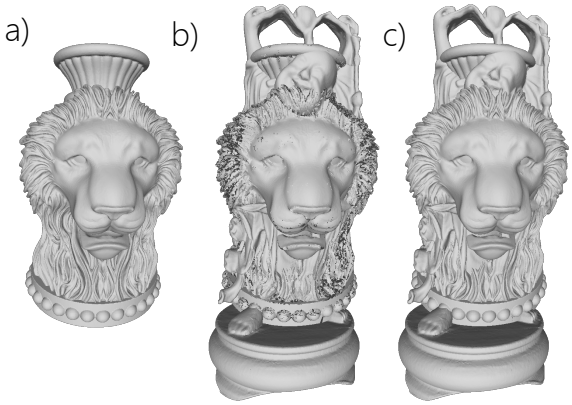

Fig. 13. Different results from $Budda \cup Lion$: a) incorrect result by CGAL, b) incorrect result by Cork, and c) correct result by our method.

computation time by caching the evaluation result during flood-filling.

The basic cache strategy is to cache final result, that is, the value of $\lambda_f(\boldsymbol{s}_i)$. We know indicator vector will not change if there is no intersection edge during propagation. That means the final classification $\lambda_f(\boldsymbol{s}_i)$ will not change, too. Thus, those faces sharing the same indicator vector can be classified as a whole.

Also, we can perform intermediate results cache. We noticed that the boolean expression can be simplified if some components of $\boldsymbol{\Lambda}(\boldsymbol{s}_i)$ is fixed. For example, assume we have a boolean expression $f = M_1 \cup (M_2 \cap M_3 - M_4)$. Given the values of two indicators $\lambda_1(\boldsymbol{s}_i) = out$, $\lambda_2(\boldsymbol{s}_i) = in$, the expression can be rewritten as $f(\lambda_1 = out, \lambda_2 = in) = out \cup (in \cap M_3 - M_4)$. Using the combination rules we can simplify the expression as $f(\lambda_1 = out, \lambda_2 = in) = P_3 - P_4$. Because for a large CSG, a certain mesh often intersects with only a few other meshes $\Theta = \{M_{n_1}, M_{n_2}, \cdots, M_{n_x}\}$. That means all the faces in this mesh has the same indicators against $M_i \notin \Theta(M_k)$. Therefore, we can first determine these fixed indicators and simplify the boolean function, and then use simplified one to compute the final indicator for each faces in this mesh.

7 Results and Discussion

We implemented the proposed method in C++ and tested a series of models on a laptop with Intel Core i5 1.5GHz CPU and 8GB RAM. To prove both the efficiency and robustness, we perform boolean evaluation on various CSGs with different complexity. We also compared our method with several previous works with available implementations, including CGAL [25], Maya [6], [40],"Cork" [41], "QuickCSG" [10], "Carve" [42], and online service of Campen and Kobbelt's plane-based method [12], [43].

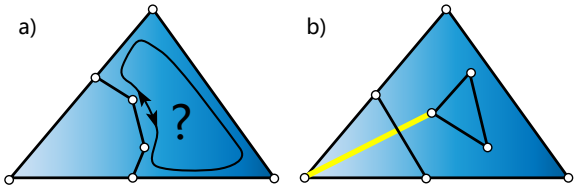

Fig. 14. a) There is ambiguity with the orientation of the loop in a tessgraph. b) When there are more than one connected component in tessgraph, we use auxiliary intersection (yellow line) to connect the two component.

7.1 Robustness & Performance

Self-union Our method is unconditionally robust for regular set mesh inputs. Even extreme degenerate cases will not lead to failure. To prove that, we tested the self-union of several examples. Table 1 shows whether the tested methods gave a valid outputs. The word 'valid' means the outputs are almost the same with the inputs. In fact, the example models *Bunny* and *Dragon* contain topology deficiencies like self-intersection that cannot perform regular set boolean operations. Despite of that, we find that our method works good in all these cases, indicating the robustness of our method. QuickCSG and Cork failed in all cases, because they cannot deal with coplanar faces. By perturbing one of the operant, the results of QuickCSG are visually OK. However, the topology of their results is messy. We can see hundreds of boundary faces on their results which do not exist in the original model (Fig. 12).

Binary boolean operations The most common situation of CSG evaluation is to perform boolean operations one by one, since many designers are used to modify models progressively. While our method can evaluate multiple boolean operations once for all, we also compared the performance of binary boolean operations to prove the efficiency. Table 2 shows the evaluation time of different methods. We can clearly see our method is very fast that is only twice as slower than the fastest non-robust QuickCSG. Other robust methods such as Maya and CGAL are much slower because they use the arbitrary precision arithmetic. Moreover, these robust methods have very strict requirements on the inputs and fragile with topology deficiencies. They simply crash when the inputs are not valid, while our method always tries to give an answer. We also noticed that in (some) very large CSGs, most time is spent on octree construction in our method. It means other stages which involve plane-based geometry take only a small percentage of time, which proves the efficiency of our plane-based algorithms*.

CSGs with large number of meshes To identify the ability of evaluating large CSG, we also test some CSG with tens or hundreds of meshes. Only QuichCSG and our

TABLE 1
Results of Self-Union Evaluation

No.	Model	Face Num.	CGAL	Maya	Cork	Carve	QuickCSG	Our Method
1	Ball	360	✓	✓	✗	✓	✗	✓
2	Head	2.7k	✓	✓	✗	✓	✗	✓
3	Bunny	70k	✗	✓	✗	✓	✗	✓
4	Dragon	277k	✗	✗	✗	✗	✗	✓

TABLE 2
Computation Time Statistics of Binary Boolean Operation (Seconds)

No.	Model	Face Num. 1	Face Num. 2	CGAL	Maya	Cork	Carve	QuickCSG	Our Method
1	Budda ∪ Lion	1.08M	400k	-	-	-	-	3.44	6.88
2	Dragon ∪ Bunny	100k	70k	-	-	-	-	0.613	1.70
3	Armadillo ∪ Armadillo2	150k	150k	487	15.4	7.00	189	0.746	1.62
4	Horse ∪ Corpse	145k	499k	-	38.6	12.6	1.52k	0.630	1.00
5	Budda ∪ Budda2	1.08M	1.08M	-	-	-	-	4.84	-

TABLE 3
Computation Time Statistics of Large CSG Evaluation (Seconds)

No.	Model	Face Num.	Mesh Num.	CGAL	Cork	Carve	QuickCSG	Our Method
1	Sprocket	11k	52	211	-	4.26	0.132	0.804
2	Ring & Ball	146k	801	-	-	187	-	62.6
3	T1	80k	50	1.00k	18.5	10.4	0.388	20.2
4	T2	7k	50	2.81k	-	16.0	0.804	-
5	H	33k	42	-	-	-	2.22	-
6	Organic	219k	6	-	14.3	63.1	0.580	2.75

method can perform multiple boolean operations directly, while others have to decompose CSG trees into binary boolean operations.. We see that the computation time of robust methods like CGAL and Maya is unacceptable long for large CSGs. On the other hand, our method keeps good performance and stability. During our experiments, we noticed sometimes Maya gives the correct results in the first few binary boolean operations, but failed in the later ones. It proves a disadvantage of incremental boolean operation methods—it could accumulate numerical errors which affects the algorithm stability.

7.2 Implementation

Searching valid loops In §5.2, we claim a valid loops on tess-graph has to be correct with its orientation. However, since tess-graph is undirectional, it is not easy to check whether a loop orientation agrees with the face's (Fig. 14a). We observe that the graph connections on the triangle edges have unambiguous directions. Starting from these edges, we can guarantee that the loops have the right orientations. After we find a valid loop, more graph connections will have unambiguous directions because one connection can participate at most two valid loops. In such way, the correct orientation will propagate in a flood-filling way.

There is another problem that the tess-graph may not be a connected graph. We avoid this problem by inserting auxiliary intersections into the tess-graph to make it connected. An auxiliary intersection links the corner vertex of triangle face (denoted as $\boldsymbol{v}_i$), which is certainly on the outer component, with the vertex on the inner component. The intersection refinement has to be performed again if the auxiliary intersections cross any other intersections. This trick slight obey the principle of no constructions. To guarantee the auxiliary intersection has a valid PBI-rep, we require the vertex from inner connected component generated by intersection between the triangle and an edge (denoted as $\boldsymbol{e}_j$) from other meshes—all intersection end points during triangle-triangle intersection are this type. In this way, we get three vertices with exact coordinates ($\boldsymbol{v}_i$ and the two end points of $\boldsymbol{e}_j$) and can construct an exact plane where the auxiliary intersection lies.

Seed indicator generation In §6.1, we claim that our flood-filling starts from a seed vertex $\boldsymbol{v}_0$. While the indicator vector of the seed $\boldsymbol{\Lambda}(\boldsymbol{v}_0)$ can be generated by point-in-polyhedron test [44] with the octree as acceleration structure [38], we have simpler strategies by using vertex with known indicators as the seed. We choose the vertex with the max x-coordinate as the seed. In this way, its indicators are either out (in, if complement is applied on mesh) or on. The on indicators are easy to determine in most time. Sometimes

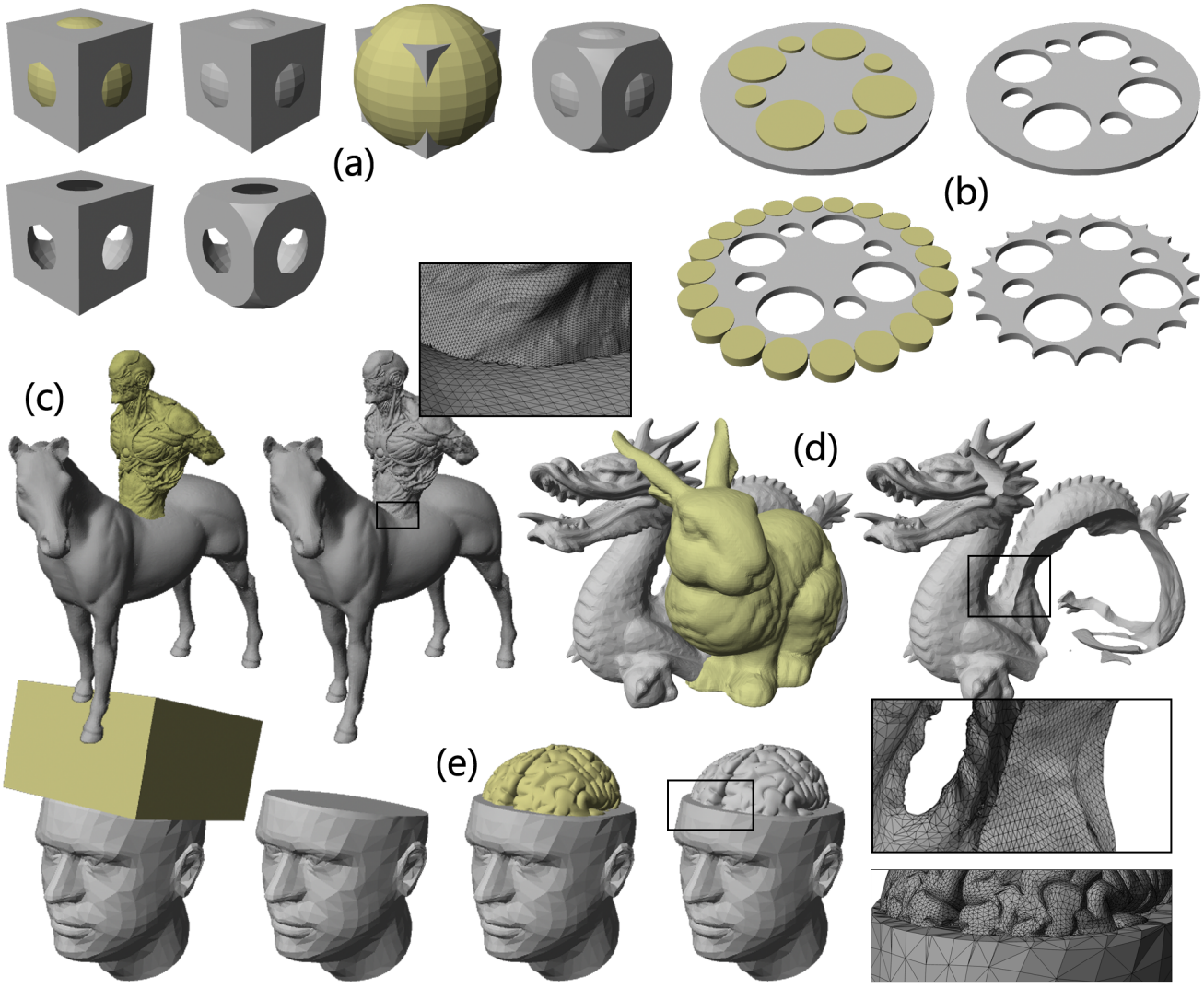

Fig. 15. **********different models: will be replaced

exception occurs because of coplanar situation—vertices may not be registered on the mesh even if it is on the mesh. Fortunately, if we carefully choose the right vertex whose neighboring faces are not coplanar, this will not happen.

The indicator vectors can propagate not only among single meshes, but can also between different meshes by the vertices and edges they share. Therefore in most time, we only need one single seed vertex for classification. However, if there are more than two connected components among meshes, we extra seeds to propagate each component. The indicators of the second and later seeds can be computed by point-in-polyhedron tests.

Exporting to float-point number The vertices of final mesh in our method are represented in either planes or vertex coordinates. While the vertices from the input meshes have there exact coordinates, the vertices newly introduced by intersection between meshes have only P-reps and require round-off when computing coordinates. Though we guarantee the correct topology in the result mesh, such round-off can still cause topology deficiencies. Here we adopt Zhou et al.'s method [7] to solve it iteratively.

7.3 Limitations and Future Work

We noticed that for CSGs that contains a lot of meshes within small area (e.g., Table. 2, *T1*), the performance of our method is poor. This is because in such situations, our method computes many intersections that will not appear as edges in the final mesh, which leads to unnecessary tessellation. Optimization may be explored to avoid such problem.

The input of our method is limited to regular set meshes. However, recent works claim that the piece-wise wind number (PWN) are more powerful to identify the inside and outside of meshes [7]. By using PWN, the input requirements can be extended to so-called PWN meshes that allow topology deficiencies such as self-intersection and multi-component. It would be interesting to extend our method to PWN method in the future.

8 SUMMARY

In this paper, we proposed a novel method to evaluate CSG models. It is able to efficiently perform unconditionally robust non-incremental boolean operations. The key idea of our approach is to embed P-reps information into B-reps. The P-reps give us the chance to strictly follow the principle of no geometry construction to avoid numerical errors. And the B-reps offer fast neighborhood query to accelerate the processing. Experiments have verified the performance of our method is competitive with state-of-the-art non-robust methods while guarantee robustness.

REFERENCES

[1] A. Requicha, "Mathematical models of rigid solid objects," 1977.

[2] R. Tilove and A. A. Requicha, "Closure of boolean operations on geometric entities," *Computer-Aided Design*, vol. 12, no. 5, pp. 219–220, 1980.

[3] C. C. Wang, "Approximate boolean operations on large polyhedral solids with partial mesh reconstruction," *Visualization and Computer Graphics, IEEE Transactions on*, vol. 17, no. 6, pp. 836–849, 2011.

[4] D. Pavić, M. Campen, and L. Kobbelt, "Hybrid booleans," in *Computer Graphics Forum*, vol. 29, no. 1. Wiley Online Library, 2010, pp. 75–87.

[5] H. Biermann, D. Kristjansson, and D. Zorin, "Approximate boolean operations on free-form solids," in *Siggraph*, vol. 1, 2001, pp. 185–194.

[6] H. Barki, G. Guennebaud, and S. Foufou, "Exact, robust, and efficient regularized booleans on general 3d meshes," *Computers & Mathematics with Applications*, vol. 70, no. 6, pp. 1235–1254, 2015.

[7] Q. Zhou, E. Grinspun, D. Zorin, and A. Jacobson, "Mesh arrangements for solid geometry," in *Tristate Workshop on Imaging and Graphics Posters*, 2016.

[8] F. R. Feito, C. J. Ogáyar, R. J. Segura, and M. Rivero, "Fast and accurate evaluation of regularized boolean operations on triangulated solids," *Computer-Aided Design*, vol. 45, no. 3, pp. 705–716, 2013.

[9] M. Segal, "Using tolerances to guarantee valid polyhedral modeling results," in *ACM SIGGRAPH Computer Graphics*, vol. 24, no. 4. ACM, 1990, pp. 105–114.

[10] M. Douze, J.-S. Franco, and B. Raffin, "Quickcsg: Arbitrary and faster boolean combinations of n solids," Ph.D. dissertation, Inria-Research Centre Grenoble–Rhône-Alpes, 2015.

[11] G. Bernstein and D. Fussell, "Fast, exact, linear booleans," in *Computer Graphics Forum*, vol. 28, no. 5. Wiley Online Library, 2009, pp. 1269–1278.

[12] M. Campen and L. Kobbelt, "Exact and robust (self-) intersections for polygonal meshes," in *Computer Graphics Forum*, vol. 29, no. 2. Wiley Online Library, 2010, pp. 397–406.

[13] K. Sugihara and M. Iri, "A solid modelling system free from topological inconsistency," *Journal of Information Processing*, vol. 12, no. 4, pp. 380–393, 1990.

[14] A. A. Requicha and H. B. Voelcker, "Boolean operations in solid modeling: Boundary evaluation and merging algorithms," *Proceedings of the IEEE*, vol. 73, no. 1, pp. 30–44, 1985.

[15] D. H. Laidlaw, W. B. Trumbore, and J. F. Hughes, "Constructive solid geometry for polyhedral objects," in *ACM SIGGRAPH computer graphics*, vol. 20, no. 4. ACM, 1986, pp. 161–170.

[16] C. Ogayar-Anguita, Á. García-Fernández, F. Feito-Higueruela, and R. Segura-Sánchez, "Deferred boundary evaluation of complex csg models," *Advances in Engineering Software*, vol. 85, pp. 51–60, 2015.

[17] S. Xu and J. Keyser, "Fast and robust booleans on polyhedra," *Computer-Aided Design*, vol. 45, no. 2, pp. 529–534, 2013.

[18] R. P. Banerjee and J. R. Rossignac, "Topologically exact evaluation of polyhedra defined in csg with loose primitives," in *Computer Graphics Forum*, vol. 15, no. 4. Wiley Online Library, 1996, pp. 205–217.

[19] S. Fortune, "Polyhedral modelling with exact arithmetic," in *Proceedings of the third ACM symposium on Solid modeling and applications*. ACM, 1995, pp. 225–234.

[20] J. Keyser, T. Culver, M. Foskey, S. Krishnan, and D. Manocha, "Esolidła system for exact boundary evaluation," *Computer-Aided Design*, vol. 36, no. 2, pp. 175–193, 2004.

[21] M. Granados, P. Hachenberger, S. Hert, L. Kettner, K. Mehlhorn, and M. Seel, "Boolean operations on 3d selective nef complexes: Data structure, algorithms, and implementation," in *Algorithms-ESA 2003*. Springer, 2003, pp. 654–666.

[22] P. Hachenberger and L. Kettner, "Boolean operations on 3d selective nef complexes: Optimized implementation and experiments," in *Proceedings of the 2005 ACM symposium on Solid and physical modeling*. ACM, 2005, pp. 163–174.

[23] S. Fang, B. Bruderlin, and X. Zhu, "Robustness in solid modelling: a tolerance-based intuitionistic approach," *Computer-Aided Design*, vol. 25, no. 9, pp. 567–576, 1993.

[24] C.-Y. Hu, N. M. Patrikalakis, and X. Ye, "Robust interval solid modelling," *Computer-Aided Design*, vol. 28, no. 10, pp. 807–817, 1996.

[25] P. Hachenberger and L. Kettner, "3D boolean operations on nef polyhedra," in *CGAL User and Reference Manual*, 4.7 ed. CGAL Editorial Board, 2015. [Online]. Available: http://doc.cgal.org/4.7/Manual/

[26] H. Bieri and W. Nef, "Elementary set operations with d-dimensional polyhedra," in *Workshop on Computational Geometry*. Springer, 1988, pp. 97–112.

[27] G. Varadhan, S. Krishnan, T. Sriram, and D. Manocha, "Topology preserving surface extraction using adaptive subdivision," in *Proceedings of the 2004 Eurographics/ACM SIGGRAPH symposium on Geometry processing*. ACM, 2004, pp. 235–244.

[28] H. Zhao, C. C. Wang, Y. Chen, and X. Jin, "Parallel and efficient boolean on polygonal solids," *The Visual Computer*, vol. 27, no. 6-8, pp. 507–517, 2011.

[29] J. Hable and J. Rossignac, "Blister: Gpu-based rendering of boolean combinations of free-form triangulated shapes," in *ACM Transactions on Graphics (TOG)*, vol. 24, no. 3. ACM, 2005, pp. 1024–1031.

[30] C. J. Ogayar, F. R. Feito, R. J. Segura, and M. Rivero, "Gpu-based evaluation of boolean operations on triangulated solids," 2006.

[31] W. C. Thibault and B. F. Naylor, "Set operations on polyhedra using binary space partitioning trees," in *ACM SIGGRAPH computer graphics*, vol. 21, no. 4. ACM, 1987, pp. 153–162.

[32] B. Naylor, J. Amanatides, and W. Thibault, "Merging bsp trees yields polyhedral set operations," in *ACM SIGGRAPH Computer Graphics*, vol. 24, no. 4. ACM, 1990, pp. 115–124.

[33] J. R. Shewchuk, "Adaptive precision floating-point arithmetic and fast robust geometric predicates," *Discrete & Computational Geometry*, vol. 18, no. 3, pp. 305–363, 1997.

[34] T. Möller, "A fast triangle-triangle intersection test," *Journal of graphics tools*, vol. 2, no. 2, pp. 25–30, 1997.

[35] L. P. Chew, "Constrained delaunay triangulations," *Algorithmica*, vol. 4, no. 1-4, pp. 97–108, 1989.

[36] L. De Floriani and E. Puppo, "An on-line algorithm for constrained delaunay triangulation," *CVGIP: Graphical Models and Image Processing*, vol. 54, no. 4, pp. 290–300, 1992.

[37] S. Gottschalk, M. C. Lin, and D. Manocha, "Obbtree: A hierarchical structure for rapid interference detection," in *Proceedings of the 23rd annual conference on Computer graphics and interactive techniques*. ACM, 1996, pp. 171–180.

[38] S. F. Frisken and R. N. Perry, "Simple and efficient traversal methods for quadtrees and octrees," *Journal of Graphics Tools*, vol. 7, no. 3, pp. 1–11, 2002.

[39] F. P. Preparata and M. Shamos, *Computational geometry: an introduction*. Springer Science & Business Media, 2012.

[40] Autodesk Ltd. (2014) Maya 2015. [Online]. Available: http://www.autodesk.com/

[41] G. Bernstein. (2013) Cork boolean library. [Online]. Available: https://github.com/gilbo/cork/

[42] T. Sargeant. (2011) Carve csg boolean library. [Online]. Available: https://github.com/VTREEM/Carve

[43] L. Kobbelt. (2010) Webbsp 0.3 beta. [Online]. Available: http://www.graphics.rwth-aachen.de/webbsp/

[44] C. J. Ogayar, R. J. Segura, and F. R. Feito, "Point in solid strategies," *Computers & Graphics*, vol. 29, no. 4, pp. 616–624, 2005.

Rui Wang is currently a postgraduate student at the Department of Computer Science and Technology, the Shanghai Jiao Tong University. His main research interests include real-time computer graphics and virtual reality applications.

Xudong Jiang received his Master degree in Computer Science from Shanghai Jiao Tong University in 2014. He is currently working in Autodesk China Research & Development Center. His research interest includes computer-aided geometric design and solid modeling.

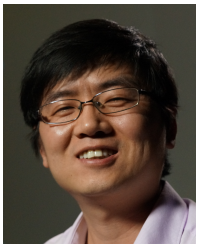

Hongbu Fu is an Associate Professor in the School of Creative Media, City University of Hong Kong. He received the PhD degree in computer science from the Hong Kong University of Science and Technology in 2007 and the BS degree in information sciences from Peking University, China, in 2002. His primary research interests fall in the fields of computer graphics and human computer interaction. He has served as an associate editor of The Visual Computer, Computers & Graphics, and Computer Graphics Forum.

Bin Sheng received his BS degree in computer science from Huazhong University of Science and Technology in 2004, MS degree in software engineering from University of Macau in 2007, and PhD Degree in computer science from The Chinese University of Hong Kong in 2011. He is currently an associate professor in the Department of Computer Science and Engineering at Shanghai Jiao Tong University. His research interests include virtual reality, computer graphics, and image-based techniques.

Enhua Wu received the BS degree from Tsinghua University in 1970, and the PhD degree from the University of Manchester (UK) in 1984. He is currently a research professor at the Institute of Software, Chinese Academy of Sciences, and Fellow of China Computer Federation. He has also been teaching at the University of Macau since 1997, where he is currently an Emeritus Professor. His research interests include realistic image synthesis, virtual reality, and scientific visualization. He has served as an associate editor of The Visual Computer, Computer Animation and Virtual Worlds.